JMEPEG (2018) 27:3276–3289
https://doi.org/10.1007/s11665-018-3422-7

1059-9495/$19.00

Synthesis, Processing and Properties of Calcium- and Nickel-Doped Yttrium Chromates(III) $Y_{0.8}Ca_{0.2}Cr_{1-x}Ni_xO_3$ (x = 0-0.3) and Studies on Their Potential Application as Coatings for SOFC Interconnects

M. Stygar, W. Tejchman, J. Dąbrowa, A. Kruk, and T. Brylewski

(Submitted February 15, 2018; in revised form April 22, 2018; published online May 29, 2018)

In the present study, a calcium- and nickel-doped yttrium chromates (YCCN)-based, conductive–protective layers for metallic interconnects used in the intermediate-temperature solid oxide fuel cells (IT-SOFCs) were investigated. Synthesis of $Y_{0.8}Ca_{0.2}Cr_{1-x}Ni_xO_3$ (x = 0; 0.15 and 0.3) powders was performed using a wet chemistry method with two different complexing agents: ethylenediaminetetraacetic acid and glycine. Based on the result of thermal analysis of obtained precursors, optimal conditions of the calcination process were determined. Powders were then milled, compacted and sintered at different temperatures using free sintering method, into series of dense, polycrystalline sinters. The use of glycine precursor allowed obtaining a single-phase material in all cases. Based on the electrical and sintering properties, the $Y_{0.8}Ca_{0.2}Cr_{0.85}Ni_{0.15}O_3$ material was selected for further studies. It was deposited using cost-effective screen-printing method on the Crofer 22APU ferritic stainless steel. To investigate properties and suitability of the resulting layer/steel system for IT-SOFCs applications, the high-temperature, dual-atmosphere studies were carried out for the first time for ceramic/metallic system, in conditions as close as possible to actual working conditions of the fuel cell. The layer exhibited high stability and good protective properties. The area-specific resistance of the studied ceramic layer/metallic substrate composite was determined, with the obtained value of 0.0366 Ω cm^2 being within the arbitrary limit set for these materials (0.1 Ω cm^2). The results show that the investigated materials are suitable for the projected application.

Keywords doped yttrium chromite, interconnect, perovskite sol–gel process, solid oxide fuel cell

1. Introduction

In the era of growing demand of worldwide energy, the solid oxide fuel cells (SOFCs) are considered to be highly promising devices that might become efficient sources of electrical energy and heat in the future. Their main advantages are very high energy conversion efficiency and relatively low emissivity, which makes them very attractive for countries characterized by highly industrialized economy, such as Japan, Germany or Scandinavian countries. The efficiency of these devices strictly depends on the properties of the applied materials and construction of the cells. Since singular fuel cell does not offer adequate voltage and current density, single cells are grouped in stacks to multiply these parameters. Materials for interconnects are chosen accordingly to very rigorous requirements such as value of thermal expansion coefficient compatible with those of the other cell's components, gas tightness, high electrical and thermal conductivity, good mechanical properties in elevated temperatures and chemical stability in the working condition of fuel cell. Due to the high-working temperatures of the cells, the first choice for materials for interconnects was lanthanum chromites materials such as $LaCrO_3$; $(La,Sr)CrO_3$; (La,Mg)-CrO_3 (Ref 1, 2). The main problems with these materials are their low gas tightness, moderate mechanical properties and very high cost of production. The reduction of SOFC operating temperatures to the 600-800 °C range made it possible to employ cost-effective metallic interconnects such as ferritic stainless steel (FSS) (Ref 3), which are currently intensively studied as potential interconnect materials for IT-SOFCs due to their low cost, ease of production and favorable mechanical properties. FSS interconnects are exposed to the aggressive environment of both air (on the cathodic side) and hydrogen/steam (on the anodic side) atmospheres in the mentioned temperature range, which severely deteriorates their electrical and mechanical properties, due to the formation of a chromia scale with low electrical conductivity on the metallic surface. In order to limit the influence of this phenomenon, ceramic-based conductive–protective layers are used (Ref 4). Their main task is to improve the electrical properties of the interconnects over the time of fuel cell action by both reducing the oxidation rate of the metallic base and increasing the electrical conductivity of the metal/ceramic system. Calcium yttrium chromate ($Y_{0.8}Ca_{0.2}CrO_3$; called YCC) and calcium–nickel-doped

Electronic supplementary material The online version of this article (https://doi.org/10.1007/s11665-018-3422-7) contains supplementary material, which is available to authorized users.

M. Stygar, J. Dąbrowa, and **T. Brylewski**, Faculty of Materials Science and Ceramics, AGH University of Science and Technology, al. Mickiewicza 30, 30-059 Kraków, Poland; **W. Tejchman**, Faculty of Geography and Biology, Pedagogical University of Cracow, ul. Podchorążych 2, 30-084 Kraków, Poland; and **A. Kruk**, Faculty of Applied IT, University of Information Technology and Management, ul. Sucharskiego 2, 35-225 Rzeszow, Poland. Contact e-mail: stygar@agh.edu.pl.

yttrium chromate ($Y_{0.8}Ca_{0.2}Cr_{1-x}Ni_xO_3$, where x = 0.15 or 0.3; called YCCN0.15 or YCCN0.3) perovskites are considered as a one of the potential types of materials with regard to such application (Ref 4). They are characterized by high physicochemical stability and adequate electrical conductivity in the operating temperatures of IT-SOFCs. The proposed composite of YCCNs layers and Crofer 22APU Ferritic Stainless Steel base should allow obtaining suitable material for SOFC interconnect, which would combine the advantages of both materials groups while minimizing their drawbacks.

Based on the available literature data (Ref 5-15), it can be said that the most important factors influencing physicochemical properties of $Y_{0.8}Ca_{0.2}CrO_3$, $Y_{0.8}Ca_{0.2}Cr_{0.85}Ni_{0.15}O_3$ and $Y_{0.8}Ca_{0.2}Cr_{0.7}Ni_{0.3}O_3$ materials are applied methods of powders preparation and conditions of sintering process. In Table 1, a short review of the methods used in synthesis of these materials is presented. As it can be seen, the most commonly applied method of synthesis of YCC and YCCN materials is the one in which glycine is used as a complexing agent in the sol–gel process.

As indicated by the previously published studies, the upper limit of doping of YCC materials with calcium is about 23-24 at.%, as introduction of Ca in higher amounts into the structures leads to the decrease in chemical stability due to the formation of additional $CaCrO_4$ phase (Ref 5). At the same time, the doping of $Y_{0.8}Ca_{0.2}Cr_{1-x}Ni_xO_3$ with nickel can be done with the x values varying from 0 to 0.2. If the x is exceeding 0.2, additional oxide phases, namely Y_2O_3 and NiO, are observed (Ref 5, 6).

In the current paper, a synthesis of YCC–YCCN compounds, with the doping amount of nickel being, respectively, x = 0; 0.15; 0.3, was conducted by means of a wet chemistry method that utilized two different complexing agents: EDTA and glycine. After optimization of sintering process, all materials were studied with respect to their electrical properties. Influence of the excess amount of Ni was investigated as well. Resulting materials were then studied in a form of coatings on the FSS substrates in the dual-atmosphere setup to simulate the actual conditions of the working fuel cell.

2. Experimental

To synthesize the ceramic powders of perovskite-type structures, two different ''soft chemical route'' methods were selected. The biggest advantages of such approach are: control over the grain size and the purity of the multicomponent systems, small variance of the grain sizes and high homogeneity of the final product.

The composite consisting of YCCNs layers and Crofer 22APU Ferritic Stainless Steel base was obtained using the screen-printing method. [The chemical composition of the used steel is presented in Ref 16] The method was chosen based on its simplicity, universality and low cost in comparison with other methods.

2.1 Powder Synthesis and Sinter Preparation

The synthesis of $Y_{0.8}Ca_{0.2}CrO_3$, $Y_{0.8}Ca_{0.2}Cr_{0.85}Ni_{0.15}O_3$ and $Y_{0.8}Ca_{0.2}Cr_{0.7}Ni_{0.3}O_3$ powders was carried out using two variants of a wet chemistry method with different chelating agents: EDTA (referred to as the ''EDTA method'') or glycine (referred to as the ''glycine method''), respectively. The procedures used to prepare the above-specified powders are illustrated in Fig. 1. Initial ingredients used for metal–organic precursors preparation were procured in the 99.99% purity grade from Sigma-Aldrich and Avantor PMP.

The obtained precursors were studied with the use of DTA–TG method (differential thermal analysis and thermogravimetry—using NETZSCH STA 449 F3) to determine optimal conditions of further thermal treatment. The samples were heated with the use of alumina crucible in a synthetic air atmosphere (10 dm^3 h^{-1} flow), with the heating rate of 10 °C min^{-1}. The experimental temperature range was 22-1050 °C.

After calcination procedure, which parameters were determined based on the DTA–TG results and XRD measurements (see section 3.1), powders were firstly dried in the room temperature and then formed into pellets, using the uniaxial pressing method in a rigid form under the pressure of 100 MPa. The final pressing was performed using cold isostatic pressing method (CIP) under the pressure of 250 MPa. After calcination, milling and compacting the powders were sintered at a temperature of 1600 °C for 1 h in air, and a number of dense, polycrystalline sinters were obtained. They were in a form of pellets of 10 mm diameter and thickness varying from 2 to 3 mm. The influence of the composition of $Y_{0.8}Ca_{0.2}Cr_{1-x}Ni_xO_3$ sinters on their physicochemical properties was analyzed based on the results of XRD, SEM–EDS and electrical conductivity measurements, with possible applications as conductive coatings considered to be the main criteria.

2.2 Preparation of the Coatings

The pastes for the screen-printing method were obtained through mixing of the chosen fine-grained perovskite powder with the organic carrier in a mass ratio of 5:1. As an organic carrier, a 5% solution of ethyl cellulose in terpineol was used. The prepared pastes then were homogenized and their viscosity was adjusted if necessary, through the content of organic support.

After obtaining, the paste was deposited on both sides of the previously prepared Crofer 22APU sample (final grinding with SiC paper grit 600; cleaning in the ultrasonic bath; cleaning with acetone). The coating was deposited using manual screen printer, with the 42-mesh screen.

Coated samples were dried for 2 h in 90 °C and then thermally annealed in the air atmosphere. The latter process was conducted in two stages. The first one was conducted at temperature of 600 °C (heating rate 1.5 °C min^{-1}), with its main goal being vaporization/burning of the organic solvent. After 1 h of isothermal annealing, the samples were cooled down to room temperature at rate of 2 °C min^{-1}. During the second stage, the samples were heated again in Ar-H_2-H_2O mixture to 1000 °C and kept in this temperature for 10 h. Finally, they were cooled down to room temperature at a rate of 5 °C min^{-1}.

2.3 Dual-Atmosphere Exposure: Experimental and Setup

The studies of the physicochemical properties of the coating/substrate layered system were conducted in single atmospheres, namely synthetic air and Ar-H_2-H_2O mixture, but also in a dual Ar-H_2-H_2O/air atmosphere setup [shown elsewhere (Ref 17, 18)], which consists of a reaction furnace, two quartz tubes (which allowed to create two different,

Table 1 Summary on the methods of powders preparation and sintering conditions of various YCC and YCCN compounds (Ref 5-15)

Authors	Compositions of perovskites $Y_{0.8}Ca_{0.2}Cr_{1-x}Ni_xO_3$	Sintering temperature, °C/time, h	Method of synthesis/ complexing agent	Results/most important properties
Yoon et al. (Ref 5)	x = 0, 0.05; 0.1; 0.15	1400-1700/12	Glycine	Conductivity of dense sinters at 900 °C in air increased from 10 to 34 S cm^{-1} with x = 0.15
Yoon et al. (Ref 6, 7)	x = 0; 0.05; 0.1; 0.15; 0.2; 0.3	1400-1700/12	Glycine	Secondary phase formation of yttrium oxide and nickel oxide was observed with higher than 20% Ni-doping
Li et al. (Ref 8)	x = 0, 0.1; 0.2	1200-1300/4	Citric acid; EDTA (ethylenediaminetetraacetic acid)	Resistance of high frequency in electrochemical impedance spectroscopy (EIS) is found to be dependent on H_2 content
Wang et al. (Ref 9)	$Y_{0.7}Ca_{0.3}CrO_3$	1400/4	Citric acid; microwave-aided sol–gel process	Pure orthorhombic perovskite phase; relative density of 96.6%
Li et al. (Ref 10)	x = 0.1	1400/4	Citric acid; EDTA	The obtained slurry was screen-printed onto both sides of YSZ or SSZ
Paulik (Ref 11)	x = 0	1600-1690/2-6 1350-1675/2-5	Glycine	Fracture toughness measured by the indentation technique decreased with increasing calcium substitution
Armstrong et al. (Ref 12)	x = 0 ($Y_{1-y}Ca_yCrO_3$; y = 0-0.4)	1400-1650/5	Glycine	Presence of $CaCrO_4$ was observed in samples with greater than 25 mol.% Ca substitution
Stevenson et al. (Ref 13)	x = 0.1 ($Y_{0.8}Ca_zCr_{0.9}Ni_{0.1}O_3$; z = 0.18-0.25)	1200-1400/2	Glycine	High purity with no detectable second phases
Jianyi (Ref 14)	x = 0.15	1350-1450/2-6	Solid-state reaction	Dense sinters
Seokgon (Ref 15)	x = 0-0.2 ($Y_{0.75}Ca_{0.25}Cr_{1-x}Ni_xO_3$)	1400/up to 10	Glycine	TEC = 10.26 × 10^{-6} [$°C^{-1}$] for x = 0.1

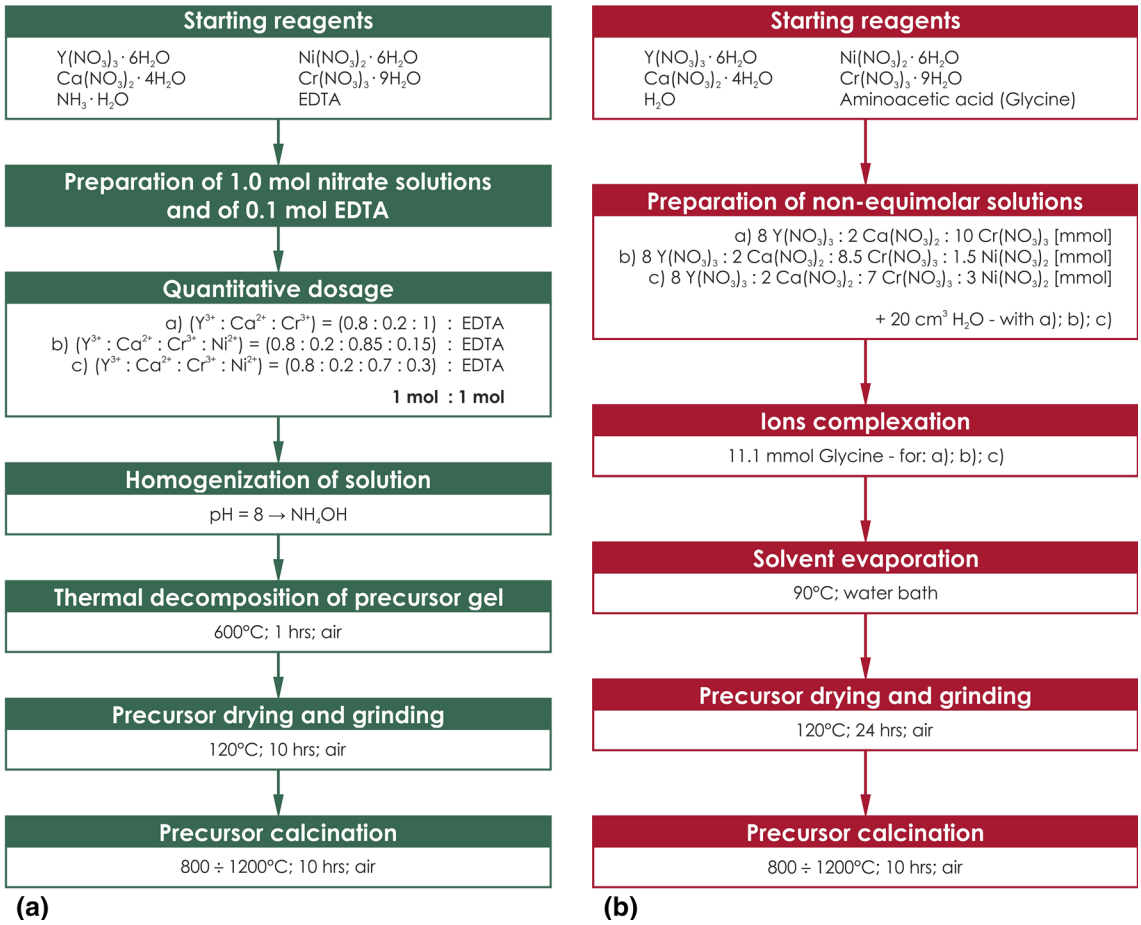

Fig. 1 Procedures used to synthesize YCCN powders via: (a) EDTA method and (b) glycine method

separate atmospheres on both sides of the examined samples), gas flowmeter system and a water vapor saturator. The most important experimental parameters for both types of investigations are presented in Table 2.

2.4 Experimental Methodology

The phase composition of the powders, bulk samples and metal–ceramics layered systems was analyzed by means of the PANalytical X'Pert Pro PW 3710 X'Celerator using CuK_α radiation, collected over a 2Θ range of 20°-90° at scan rate of 0.008° and 80 s. count. Qualitative and quantitative analyses of the samples' compositions were conducted using X'Pert HighScore Plus 2.0, Crystal Impact—Match!2 and CrystalDiffract® 6.0.5. (with PDF-2 ICDD database) software. Scanning electron microscopy (FEI Nova NanoSEM 200; JEOL JSM-6610LV) coupled with an EDAX Genesis XM x-ray microanalysis system was used to examine the morphology and chemical composition of the studied samples. The rheological characterization of YCC-YCCN powders was performed based on the grain size distribution and BET specific surface area measurements (Brunauer–Emmett–Teller—using Nova 1200e Quantachrome Instr., adsorption of nitrogen). The electrical conductivity of the sinters and electrical resistance of coated steel were measured using the DC 2-probe 4-point- HP 34401A multimeter with a constant current of 10 mA and within temperature range: 500-800 °C for sinters and coated/uncoated steels, and, in addition, at 800 °C in the case of long-term (200 h) measurements taken for coated/uncoated steels. The electrical resistance of oxidized coated/uncoated steels is usually measured in terms of its area-specific resistance (ASR), which is defined as the product of resistance and nominal contact surface area of the oxide and steel. Due to the symmetrical design of the test, the area-specific resistance of the samples was calculated based on the obtained resistance values using the following formula:

$$\mathrm{ASR} = \frac{R \cdot A}{2} \qquad \text{(Eq 1)}$$

where R—electrical resistance [Ω], and A—surface area of the Pt layer [cm^2].

Samples for long-term ASR measurements were separately oxidized before the measurements for 50 h at temperature of 800 °C [which was explained elsewhere (Ref 19)]. For this kind of examination, both sides of sinters and composite systems were coated with Pt paste using screen-printing. The apparatus and the methods used for measuring electrical resistance are described in Ref 20. The sinters were also investigated using electrochemical impedance spectroscopy (EIS) method. In this case, the measurements were conducted in the air atmosphere at temperatures varying from 25 to 800 °C, using potentiostat–galvanostat Metrohm AutoLab type PGSTAT302 N in a frequency range 1 mHz to 1 MHz. During measurement, the thermodynamic equilibrium was assumed, with the values of resistance being constant in a function of time at given temperature.

Table 2 Experimental conditions of studies in both single and dual atmospheres

Parameter	Single atmosphere	Dual atmosphere
Substrate material	Crofer 22APU [W.-No. 1.4760 X1CrTiLa22 —DIN EN standard; UNS S44535—ASTM standard)]; ThyssenKrupp VDM GmbH; Germany	
Substrate specimen shape	Steel coupons in the form of disks; ø 10 mm; 1 mm thickness	Steel coupons in the form of disks; ø 28 mm; 1 mm thickness
Surface treatment of substrate	Grinding with 100-600-grid SiC papers; ultrasonically degreasing and washing in acetone and ethanol	
Reaction temperature	800 °C	
Exposure time	100; 250 h	250 h
Atmosphere	Ar-10%H_2-H_2O (ratio of partial pressures $p(H_2/pH_2O)$ = 94/6) or Synthetic air (partial pressure of oxygen $p(O_2)$ = 0.21 atm)	Ar-10%H_2-H_2O left side/right synthetic air (ratio of partial pressures $p(H_2/pH_2O)$ = 94/6 with partial pressure of oxygen = 0.21 atm)

3. Results and Discussion

3.1 Optimization of Calcination Parameters

The results of the DTA–TG measurements are shown in Fig. 2. Based on the shape of obtained TG curves (Fig. 2a), all organic precursors, obtained with the use of EDTA as chelating agents, decomposed into the desired compounds with overall weight loss of approximately 90 wt.%. Small endothermic effects suggest loss of water at the early stages of heating, while the presence of big, exothermic peaks could be related to the oxidation of the organic precursors. The weight did not change any further in case of all examined samples, after occurrence of the last exothermic peak in the range of 300-340 °C.

In the case of compounds obtained with the usage of glycine (Fig. 2b), all samples were dried out for 24 h in 120 °C to remove the water from the hydrated coordination complexes. The DTA of these samples was conducted directly after the drying process, due to their highly hygroscopic properties. In the temperature range of 153-180 °C for each of the examined compounds, a single exothermal peak is observed, which position is strongly correlated with the drastic loss of mass observed on the TG curve. However, it should be noted that the loss of mass in each case continued up to a temperature of about 600 °C. The total mass loss in the samples obtained by glycine method varies from 73 to 79%.

Based on the DTA–TG results, optimal conditions of thermal treatment for precursors obtained by both described methods were found. For the precursor obtained by means of the glycine method, it was necessary to use temperatures in excess of 600 °C. In the case of precursor obtained by EDTA method, the optimal thermal conditions were found to be higher than 350 °C.

The choice of optimal calcination parameters was based on the result of XRD phase composition studies of samples calcinated for 10 h in temperatures: 800, 900, 1000, 1100 and 1200 °C. Materials with the Ni content x = 0 and 0.15 obtained via glycine method were found to be stable in the temperature range of 800-1200 °C, exhibiting single-phase structure. In the material with x = 0.3, additional Y_2O_3 and NiO phases were detected. In the case of materials obtained using EDTA method, the samples with x = 0.15 and 0.3 were found to be unstable. The detailed discussion of these results is presented in section 3.1. For further studies, powders calcinated in 1200 °C (materials for sintering) and 1000 °C (materials for coatings) were selected, with the latter value being dictated by reaching the limit of free sintering (Ref 6).

3.2 Morphology Characterization and XRD Phase Structure Analysis

In order to obtain information on the shape and size of grains and their degree of agglomeration in powders with a perovskite structure, observations of their morphology were made using scanning electron microscopy as shown in Fig. 3.

SEM micrographs of the $Y_{0.8}Ca_{0.2}Cr_{x-1}Ni_xO_3$ (x = 0; 0.15; 0.3) powders, obtained with the use of EDTA method and calcinated at 1200 °C for 10 h, show the presence of two different types of grains: spherical grains of diameter smaller than 1 μm, which exhibit tendency toward the formation of big, porous agglomerates of diameters of tens of micrometers, and needle-like grains, most probably of β-$CaCr_2O_4$ phase (Fig. 3a, b, and c). On the other hand, the powders obtained with the use of the glycine method and after similar thermal treatment as in the previous case consisted only of spherical grains, with their diameter in the range of 0.29-1.33 μm (Fig. 3d, e, and f). What is more, in the powders obtained with the use of glycine a macroscopic change in morphology can be observed, which indicates the start of the sintering process.

In Table 3, the results of the BET specific surface area measurements, crystalline size based on the XRD results [estimated with the use of Scherrer equation (Ref 21)] and the size of grains estimated from the SEM observations are summarized, for materials obtained by both EDTA and glycine methods and calcinated at 1200 °C for 10 h in air.

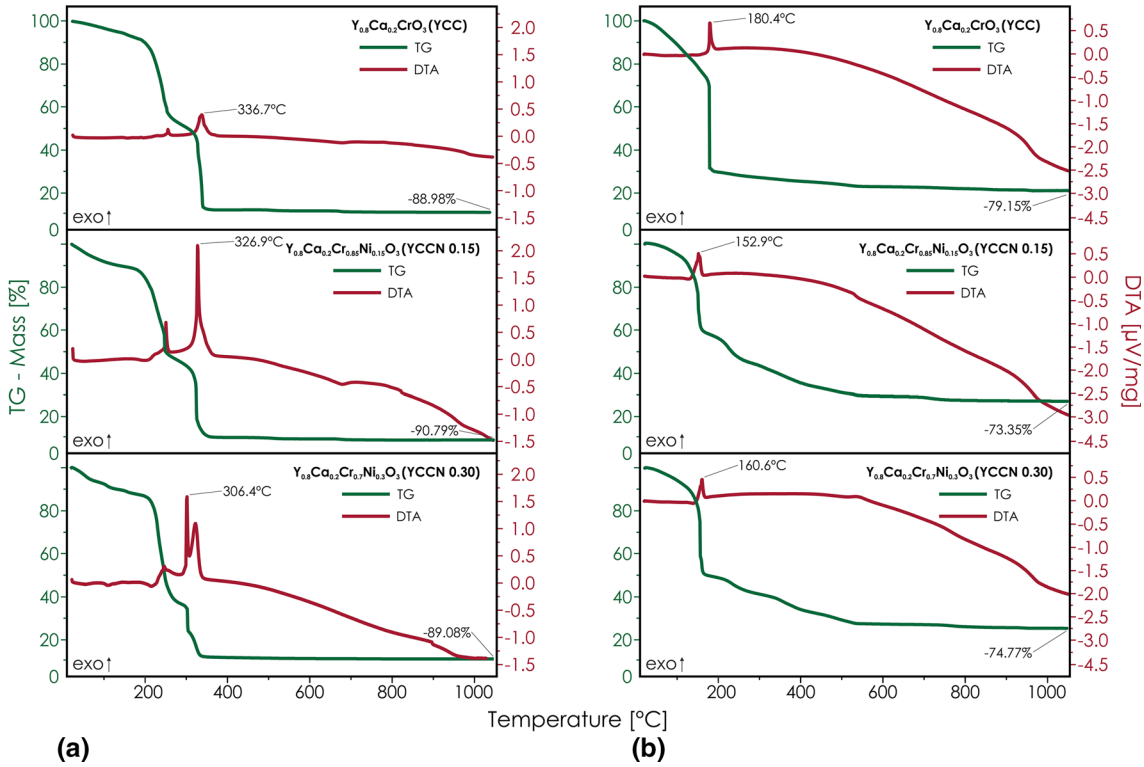

Fig. 2 DTA–TG curves obtained for precursors synthesized via: (a) EDTA method and (b) glycine method

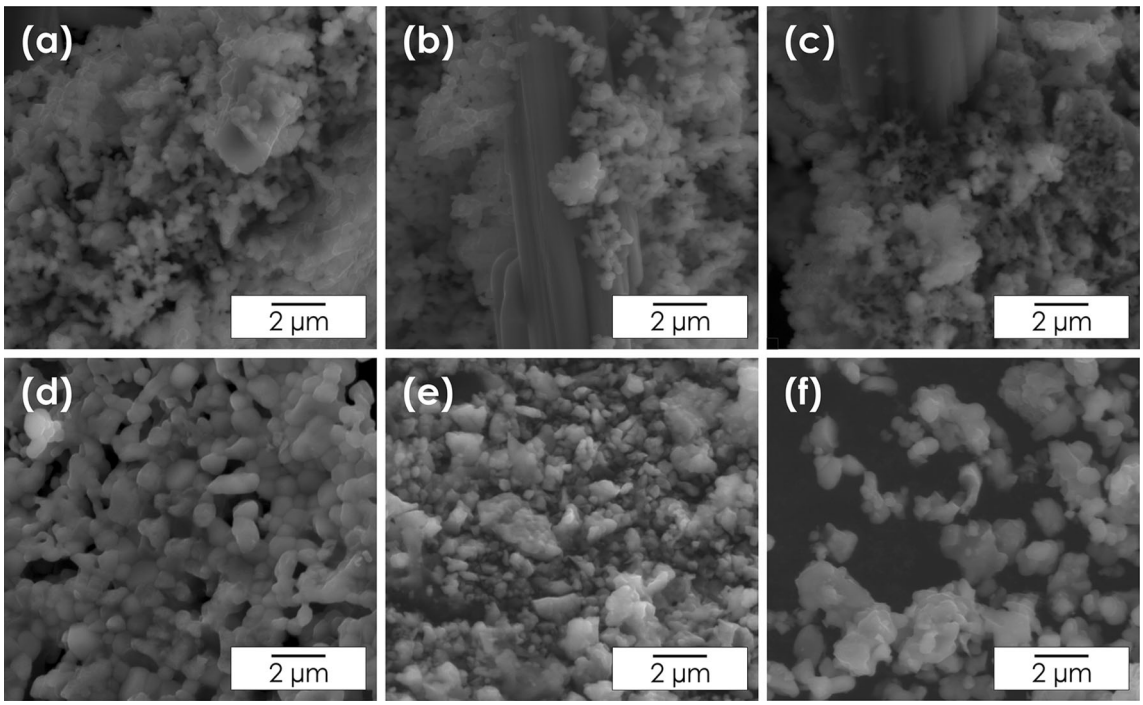

Fig. 3 SEM micrographs of $Y_{0.8}Ca_{0.2}Cr_{1-x}Ni_xO_3$ powders synthesized and calcinated at 1200 °C using: the EDTA method—for (a) $x = 0$, (b) $x = 0.15$, (c) = 0.3, and the glycine method—for (d) $x = 0$, (e) $x = 0.15$, (f) = 0.3 (mag. 1000×)

The calculated crystallite size with a minimum of 20 reflections assigned to the $YCrO_3$ phase for each sample is in the range from 34 to 50 nm, with the typical size for the majority of measurements being around 48 nm. The relatively high degree of variation in the value of single measurements of crystallite sizes, especially for the EDTA method, indicated the deviation from the spherical shape of the crystallites.

The morphologies of the sinters obtained from powders prepared by means of both EDTA and glycine methods and

subjected to 1 h of thermal treatment in air at 1600 °C are presented in Fig. 4. As it can be seen, in the case of sinters synthesized with EDTA method, fraction of grains of considerably larger size was present, which is especially evident in Fig. 4(b). This may be an indication that more than one phase occurred within the system. The sinters obtained using glycine method exhibited completely different morphologies in comparison with the previously described polycrystalline materials (Fig. 4d, e, and f).

Independent of the nominal chemical compositions, all materials obtained using the glycine method had well-developed grains of characteristic isometric shape. What is more, in contrast to the previous group of sinters, in this case only a few inter-agglomerate pores were observed. On the surface of the $Y_{0.8}Ca_{0.2}Cr_{0.7}Ni_{0.3}O_3$ sinter (Fig. 4f), additional irregular crystals (probably NiO phase) were sporadically observed.

The observed higher grain refinement of the sinters obtained using the glycine method was slightly surprising considering the results of specific surface area BET measurements, which indicated that the powders obtained by EDTA methods are characterized by larger surface area (in the range of 2.28 ± 0.07 to 6.69 ± 0.04 m^2 g^{-1}), while the value for the powders obtained for glycine method was in the range of 1.57 ± 0.06 to 3.99 ± 0.04 m^2 g^{-1}. The main reason for such discrepancy can be attributed to the tendency of fine powders, obtained by glycine method, toward agglomeration, which was confirmed by SEM observations.

Figure 5 shows the diffraction patterns for powders calcinated for 10 h in air at 1200 °C and for sinters obtained from these powders, sintered for 1 h in air at 1600 °C. Based on the ex situ phase analysis of powders obtained by means of EDTA method, it can be said that all examined materials exhibited multiphase composition (Fig. 5a). The main phase observed in all materials synthesized by both methods was the orthorhombic $YCrO_3$ one (Fig. 5a and b). Besides, the following phases were also identified: NiO (in compounds with $x = 0.3$, a result of substitution limit for nickel), tetragonal $CaCr_2O_4$ and orthorhombic β-$CaCr_2O_4$.

The explanation of the presence of $CaCr_2O_4$ in two different phases may be analogical to the one presented by Armstrong et al. (Ref 12) for similar compounds in reducing atmosphere. The $CaCrO_4$ phase, which at temperatures in excess of 1000 °C is a liquid one, may decompose into two different $CaCr_2O_4$ phases, which is shown in the following equation:

$$4CaCrO_4 + 2Cr_2O_3 = 4(\alpha, \beta) - CaCr_2O_4 + 3O_2 \qquad \text{(Eq 2)}$$

Both $CaCr_2O_4$ phases, which presence is unfavorable from the point of view of electrical conductivity (especially the β phase), decomposed during sintering in 1600 °C. In the case of the compound undoped by nickel, the decomposition/desolution of $CaCr_2O_4$ phases was practically complete. In the case of compound with nickel content of $x = 0.15$, a partial decomposition was observed, while for the compound with $x = 0.3$ no visible changes were recorded. This situation is especially interesting, as in the temperature range of 1570-1600 °C a phase transformation of $CaCr_2O_4$ from orthorhombic (β) to tetragonal (α) phase is reported (Ref 22, 23).

The occurrence of additional phases in compounds synthesized using the EDTA method is rather surprising, considering the number of successful synthesis of other similar perovskites and spinels [e.g., $Mn_{1+x}Co_{2-x}O_4$ (x = 0-1.5) (Ref 24); $La_{0.8}Ca_{0.2}CrO_3$ and $La_{0.6}Sr_{0.4}CoO_3$ (Ref 25); $La_{0.8}Sr_{0.2}CrO_3$ (Ref 26); $Cu_{0.3}Mn_{1.1}Co_{1.8}O_4$ (Ref 27)]. The most probable reason of observed phenomenon seems to be a trouble with keeping the pH of the solution on a steady value of 8 despite constant addition of ammonia during the process. This may indicate that these compounds are extremely vulnerable to even small deviations from the optimal conditions of pH.

Similarly to the results obtained by Yoon et al. (Ref 5-7), both powders and sinters obtained using glycine method were characterized by orthorhombic structure. Based on the results of XRD analysis (Fig. 5b), it can be said that the pure $YCrO_3$ phase occurred only for the compound with nickel content $x = 0.15$. For the material without nickel ($x = 0$) additionally a Y_2O_3 was found, and for the case of $x = 0.3$ both Y_2O_3 and NiO were present in both powders and sinters [which was explained elsewhere (Ref 13)].

It should be noted that the substitution of the trivalent chromium ion with divalent nickel ion does not influence values of the lattice constant of the $Y_{0.8}Ca_{0.2}Cr_{1-x}Ni_xO_3$ (x = 0; 0.15 and 0.3) compounds and as a result does not influence the volume of primitive cell. This phenomenon can be explained by similar ionic radius of both Cr^{3+} (0.62Å) and Ni^{2+} (0.69Å) ions. Yoon et al. suggested (Ref 5) that another important factor may be a partial substitution by trivalent nickel ion of low spin configuration ($t_{2g}^6 e_g^1 (s = 1/2)$). Such compensating mechanism explains why the differences in lattice constants are so small, that even XRD methods do not allow detecting them.

Table 3 Results of the BET specific surface area measurements, crystalline size based on the XRD results and the size of grains estimated from SEM micrographs of the studied powders

	Mass fraction, %		
Physicochemical parameter	**Ni = 0.0**	**Ni = 0.15**	**Ni = 0.3**
Powders synthesized via EDTA method			
BET specific surface area, m^2 g^{-1}	4.64 ± 0.06	2.28 ± 0.07	6.69 ± 0.04
Average size of crystallites—$YCrO_3$ [nm]	46.0	47	49
Estimated grain size—$YCrO_3$, μm	0.29-0.61	0.20-0.60	0.14-0.80
Powders synthesized via glycine method			
BET specific surface area, m^2 g^{-1}	1.57 ± 0.06	1.86 ± 0.051	3.99 ± 0.04
Average size of crystallites, nm	49	49	50
Estimated grain size, μm	0.57-1.33	0.29-1.30	0.62-0.91

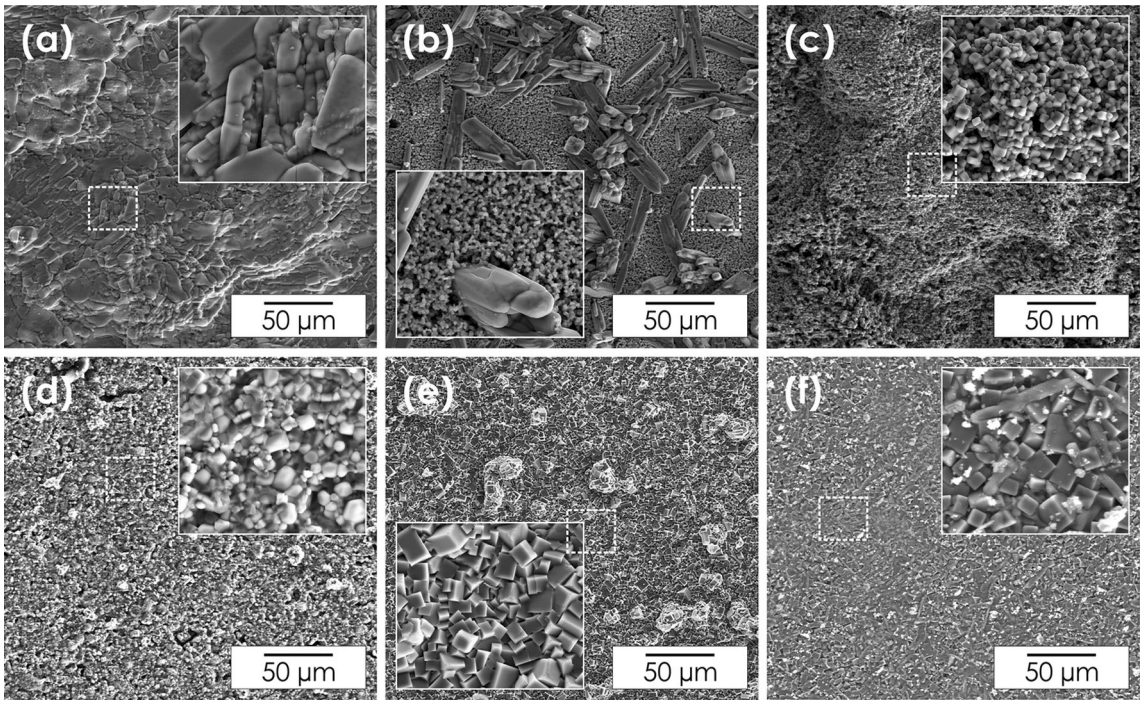

Fig. 4 SEM micrographs of $Y_{0.8}Ca_{0.2}Cr_{1-x}Ni_xO_3$ sinters obtained from powders synthesized using EDTA method: (a) $x = 0$; (b) $x = 0.15$; (c) = 0.3; and glycine method: (d) $x = 0$; (e) $x = 0.15$; (f) = 0.3(mag. 1000x)

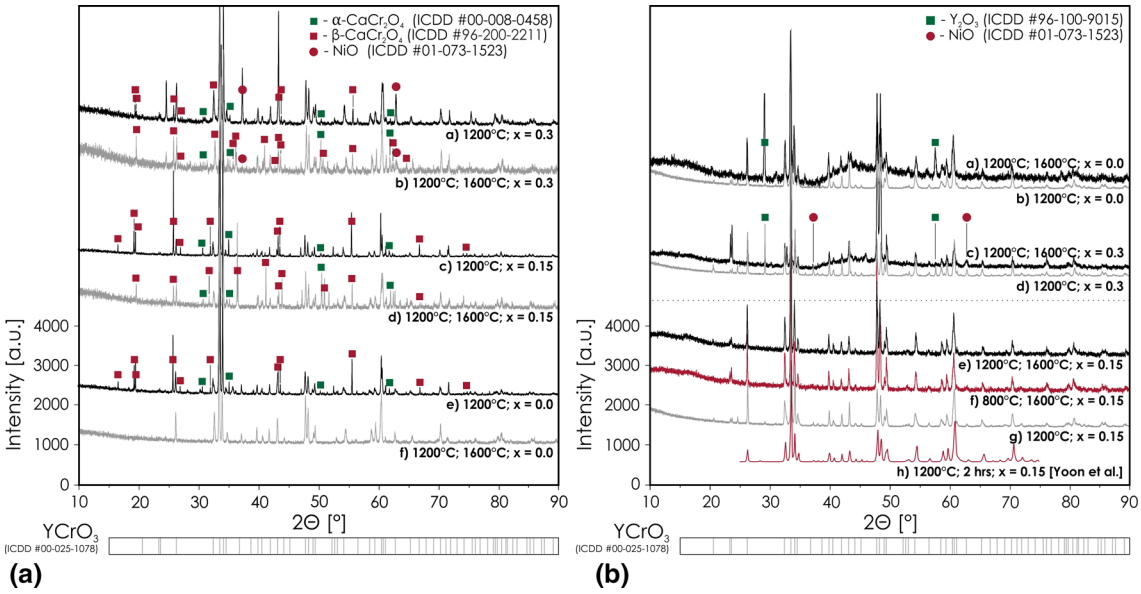

Fig. 5 XRD spectra of powders and sinters synthesized via: (a) EDTA method and (b) glycine method (Ref 5)

Using the relation between intensity of refracted beams and quantity of the given phase in the measured sample, a content of each phase in all examined compositions of $Y_{0.8}Ca_{0.2}Cr_{1-x}Ni_xO_3$ powders, calcinated for 10 h in 1200 °C in air atmosphere, was evaluated using software for phase identification mentioned before. The results are presented in Table 4.

3.3 Electrical Properties

The studies conducted using DC 2-probe 4-point technique revealed that the electrical conductivity of all sinters increased with the temperature increase, confirming their semiconducting character. At the temperature of 800 °C, which is close to the working conditions of SOFCs, the sample characterized by the highest electrical conductivity of 50.3 $S{\cdot}cm^{-1}$ was $Y_{0.8}Ca_{0.2}Cr_{0.85}Ni_{0.15}O_3$ sinter, obtained based on the powders synthesized by the glycine method. At the same time, the worst electrical properties were observed in the samples undoped by Ni, with the value of electrical conductivity measured for the sinter, obtained using the same method as in the previous case, being 11.9 $S{\cdot}cm^{-1}$.

In Fig. 6, the temperature dependence of the electrical conductivity of all examined $Y_{0.8}Ca_{0.2}Cr_{1-x}Ni_xO_3$ sinters (x = 0; 0.15; 0.3, both methods of synthesis, calcination for 10 h at 1200 °C, sintering for 1 h at 1600 °C) is presented.

Using the Arrhenius relation for the electrical conductivity in a form presented below, it was possible to calculate the activation energy of the process:

$$\sigma = \left(\frac{\sigma_0}{T}\right) \exp\left(\frac{-E_a}{kT}\right) \quad \text{(Eq 3)}$$

where σ—electrical conductivity of the sinter [Ω^{-1} cm^{-1}]; σ_o—pre-exponential factor [Ω^{-1} cm^{-1} K^{-1}]; E_a – energy of activation [eV]; k—Boltzmann's constant [eV K^{-1}].

Table 4 Mass fraction of each phase in the $Y_{0.8}Ca_{0.2}Cr_{1-x}Ni_xO_3$ powders with x = 0; 0.15 and 0.3 calcinated for 10 h in air at 1200 °C

	Mass fraction, %		
Identified phase	**Ni = 0.0**	**Ni = 0.15**	**Ni = 0.3**
Powders synthesized via EDTA method			
$YCrO_3$	30.2	25.5	43.2
α-$CaCr_2O_4$	20.4	17.4	17.1
β-$CaCr_2O_4$	49.4	57.1	31.1
NiO	…	…	8.6
Identified reflexes, %	96.6	92.8	94.9
Powders synthesized via glycine method			
$YCrO_3$	99.1	100	98.6
Y_2O_3	0.9	…	0.9
NiO	…	…	0.5
Identified reflexes, %	99.6	99.5	99.1

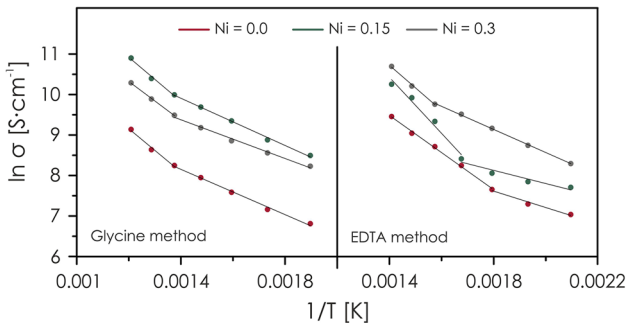

Fig. 6 Temperature dependence of electrical conductivity for $Y_{0.8}Ca_{0.2}Cr_{x-1}Ni_xO_3$ (x = 0; 0.15 and 0.3) sinters obtained by both EDTA and glycine methods presented using Arrhenius plot

After taking the logarithm of both sides of Eq 3, a following equation is obtained:

$$\ln \sigma T = -\frac{E_a}{k} \cdot \frac{1}{T} + \ln \sigma_0 \quad \text{(Eq 4)}$$

Presenting the data using the Arrhenius plot, the slope of the line (equal to E_a/k in this case) was estimated using the linear regression. Based on this, the energies of activation for each case were found. In all cases, measuring error of energies of activation does not exceed 0.01 eV. Their values are presented in Table 5.

As it can be seen, the values of activation energy at temperatures below 700 °C are significantly lower than for temperatures higher than 700 °C, with the exception of the two sinters that had been obtained via the EDTA method and had compositions corresponding to x = 0 and 0.3. This may be a result of the change in the electrical conductivity mechanism, for example, from the grain boundary mechanism to the conduction through the bulk of the grains. In general, the first type is characterized by lower energies of activation and occurs in the low temperature range, which is in agreement with the presented results. Furthermore, it can be seen that in the case of EDTA, a change in the activation energy is associated with increasing nickel content.

To the further studies, including the test of coating/metallic substrate layered systems, only the $Y_{0.8}Ca_{0.2}Cr_{0.85}Ni_{0.15}O_3$ compound was selected, due to its preferable electrical properties. While at this stage it was clear that the sinter obtained using glycine method was characterized by better properties, both sinters of this type were further investigated for comparison.

The studies using electrochemical impedance spectroscopy method (EIS) were conducted on both $Y_{0.8}Ca_{0.2}Cr_{0.85}Ni_{0.15}O_3$ sinters, prepared by both previously described methods (EDTA and glycine), calcinated for 10 h in 1200 °C and sintered for 1 h in 1600 °C. The data were analyzed using the equivalent circuit method, which allowed extracting the basic electrical properties and separating contributions of different phases. Firstly, the form of equivalent circuit was proposed; then, using the optimization methods (least square errors + conjugate gradients) parameters of each electrical element were determined. The applied equivalent circuit allowed very close approximation of the experimental data.

In Fig. 7(a), an exemplary set of spectra, measured at low and medium temperatures for the sample obtained using EDTA method, is presented. In this case, the equivalent circuit was postulated in a form of series circuit of two parallel RC connections. Additional resistor was added to compensate for the resistance of the experimental setup. (The capacity effect was deemed to be negligible.) Each RC circuit was used to

Table 5 Activation energy of electrical conductivity determined for the examined sinters

$Y_{0.8}Ca_{0.2}Cr_{x-1}Ni_xO_3$	Activation energy [eV] in a given temperature range [°C]					
	500÷550	**550÷600**	**600÷650**	**650÷700**	**700÷750**	**750÷800**
x = 0.0 (EDTA method)	0.75		0.39			
x = 0.15 (EDTA method)	0.25				0.48	
x = 0.3 (EDTA method)	0.14			0.59		
x = 0.0 (glycine method)	0.24				0.46	
x = 0.15 (glycine method)	0.25				0.47	
x = 0.3 (glycine method)	0.21				0.41	

mimic the properties of a different phase: the first one described properties of $YCrO_3$ and the second of $CaCr_2O_4$. Such interpretation is also consistent with the result of XRD, which showed that both these phases coexist in the measured sample.

In the case of the sinter, based on the glycine method obtained powders, analogical studies were conducted. The exemplary spectra for this sample are presented in Fig. 7(b). In this case, an extremely simple equivalent circuit was postulated, in a form of series connection of resistor (describing properties of the experimental setup) and parallel RC circuit (sample's properties), giving an excellent fit quality. The EIS results confirmed the results of XRD analysis, showing that only one main phase is present in the sample, namely the $YCrO_3$.

Based on the obtained data and using Eq 4, the electrical conductivity was calculated for each phase in both studied samples. Using the Arrhenius relation (Eq 2), the energies of activation were calculated for each phase. The results are presented in Fig. 7 and summarized in Table 6.

The obtained values of energies of activation show the importance of the base $YCrO_3$ perovskite phase in terms of general electrical properties of the examined compounds, as well as the inferior electrical properties of $CaCr_2O_4$ phase.

3.4 General Properties of the Conductive–Protective Coating System

To obtain dense, uniform coating, a screen-printing method, combined with the suitable thermal treatment, was used. The details are described in section 2.2. After deposition on the metallic substrates, all coatings were characterized by good macroscopic properties: uniformity of thickness and color, as well as lack of cracks.

The main part of studies was conducted in a condition close to the working environment of the solid oxide fuel cells to properly assess the potential of the investigated materials in the role of conductive–protective coatings. The oxidation tests were carried out in dual-atmosphere setup at temperature of 800 °C for 250 h. It should be noted that to the best of authors' knowledge, this was the first time when dual-atmosphere studies were conducted on the layer/steel system instead of studies on the pure metallic substrate.

Despite the presence of high gradients of chemical potential of both oxygen and hydrogen, no significant structural changes were observed within the layer or on the coating/substrate interface. The XRD results shown in Fig. 8(a) clearly indicate the lack of phase transitions and single-phase structure within the whole volume of coating.

Studies of morphology combined with the EDS results, which are visible in Fig. 8(b), (c), (d), and (e), confirmed good agreement between the obtained composition and the nominal one, namely $Y_{0.8}Ca_{0.2}Cr_{0.85}Ni_{0.15}O_3$. Supplementary Fig. 10 (included in a separate document) shows the EDS line scan profile from the sample annealed for 250 h at 800 °C in a dual atmosphere corresponding to the air side of a SOFC. Results are consistent with the results of EDS point measurements.

The observed structure was characterized by relatively high porosity and consisted mainly of irregularly shaped grain agglomerates of size 5-15 μm. Based on the SEM observations,

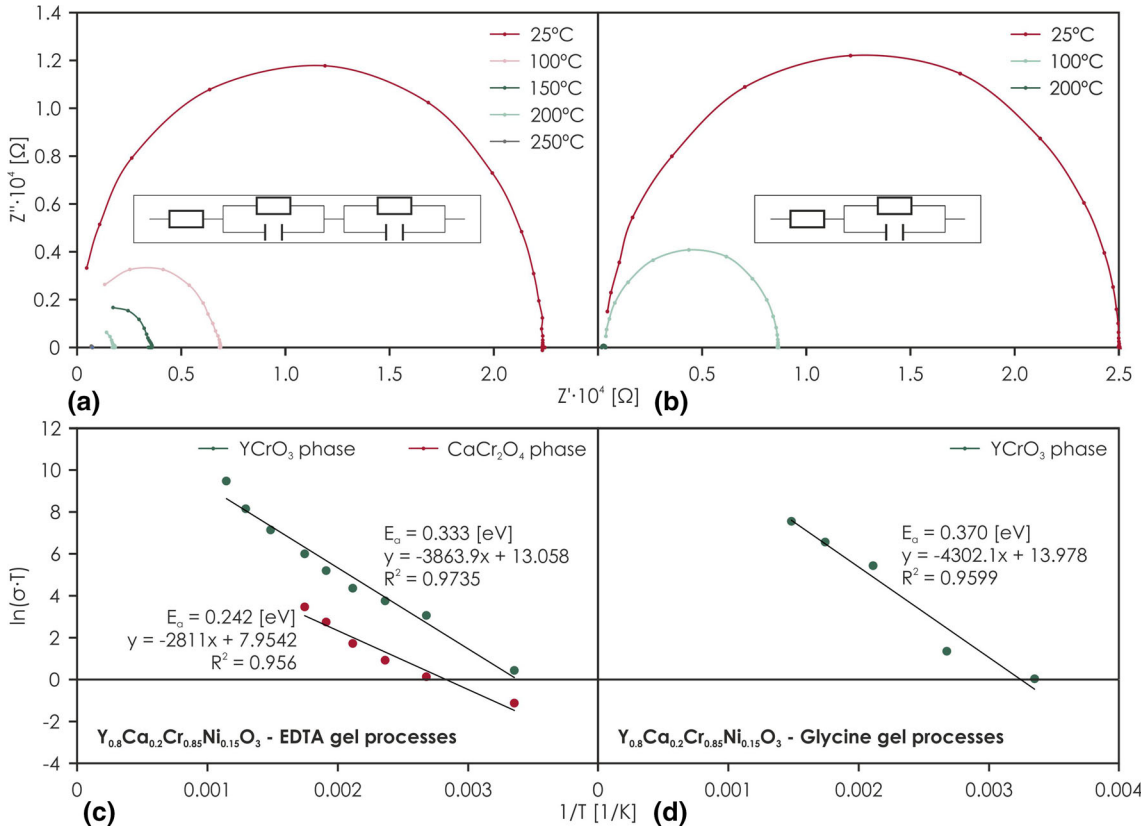

Fig. 7 Examples of impedance spectra and temperature dependence of electrical conductivity measured for $Y_{0.8}Ca_{0.2}Cr_{0.85}Ni_{0.15}O_3$ sinters obtained from powders prepared via: (a), (c) EDTA method; and: (b), (d) glycine method

Table 6 Activation energy of electrical conductivity measured for $Y_{0.8}Ca_{0.2}Cr_{0.85}Ni_{0.15}O_3$ sinters

	Activation energy of electrical conductivity [eV] with the value of measurement error			
	$YCrO_3$ phase		$CaCr_2O_4$ phase	
EDTA method	0.33	± 0.02	0.24	± 0.04
Glycine method	0.37	± 0.03	…	…

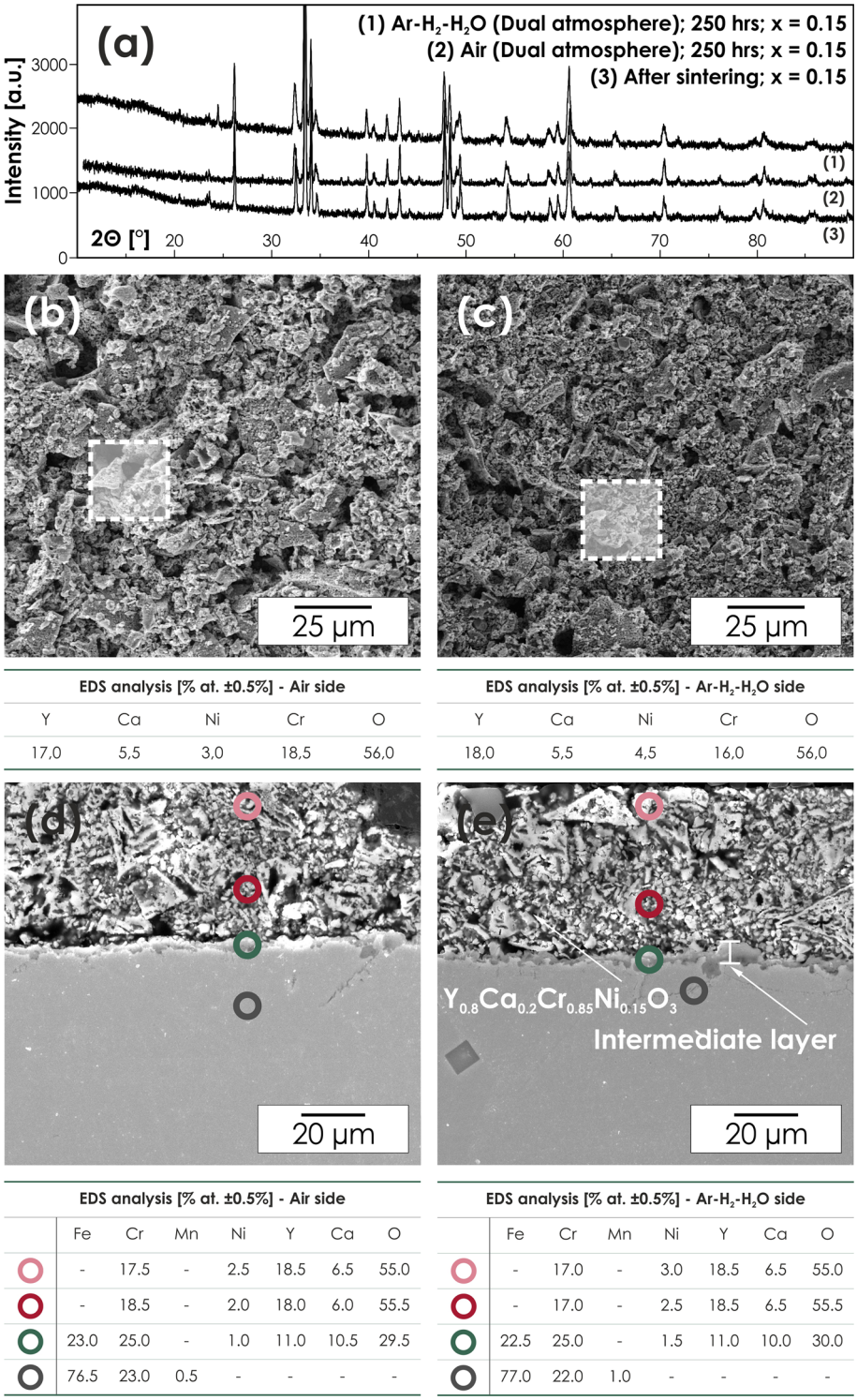

EDS analysis [% at. ±0.5%] - Air side

Y	Ca	Ni	Cr	O
17,0	5,5	3,0	18,5	56,0

EDS analysis [% at. ±0.5%] - Ar-H_2-H_2O side

Y	Ca	Ni	Cr	O
18,0	5,5	4,5	16,0	56,0

EDS analysis [% at. ±0.5%] - Air side

	Fe	Cr	Mn	Ni	Y	Ca	O
○	-	17.5	-	2.5	18.5	6.5	55.0
○	-	18.5	-	2.0	18.0	6.0	55.5
○	23.0	25.0	-	1.0	11.0	10.5	29.5
○	76.5	23.0	0.5	-	-	-	-

EDS analysis [% at. ±0.5%] - Ar-H_2-H_2O side

	Fe	Cr	Mn	Ni	Y	Ca	O
○	-	17.0	-	3.0	18.5	6.5	55.0
○	-	17.0	-	2.5	18.5	6.5	55.5
○	22.5	25.0	-	1.5	11.0	10.0	30.0
○	77.0	22.0	1.0	-	-	-	-

Fig. 8 XRD analysis of the YCCN layers after 250 h of annealing in a dual atmosphere at 800 °C (a). Morphology and cross-sectional micrographs with EDS analysis: (b), (d) air side and (c), (e) Ar-H_2-H_2O side

the size of grains was estimated to be between 0.1 and 0.8 μm (Fig. 8d and e).

The appliance of screen-printing method resulted with thick, porous layer characterized by good adhesion to the metallic substrate. Observations of the cross sections of coating/substrate systems oxidized in dual-atmosphere conditions allowed to determine the thickness of the ceramic coating after the process, with the values varying from 60 to 100 μm (Fig. 8d and e). The obtained thickness, while relatively big, is typical for conductive–protective layers obtained by screen-printing method (Ref 27). On the coating/substrate interface, an additional intermediate layer was observed, of thickness varying from 1.7 to 7.6 μm. Beneath this layer, no signs of internal oxidation or oxide's precipitations were observed, which are characteristic for the uncoated Crofer 22APU steel. EDS analysis revealed that this reactive layer consisted mostly of Fe, Y, Ca and Cr, with the oxygen being present as well.

Similar intermediate layers were observed in, e.g., $Mn_{1.5}Co_{1.5}O_4$/AL453 or $Cu_{0.3}Mn_{1.1}Co_{1.8}O_4$/DIN 50049 systems. In these cases, the intermediate layer was formed as a result of chemical reaction between the coating and chromium from the metallic substrate. The presence of intermediate layer increased the adhesion of the coating, as well as improved electrical properties of the whole system (Ref 27, 28). It is possible that in our case analogical processes took place.

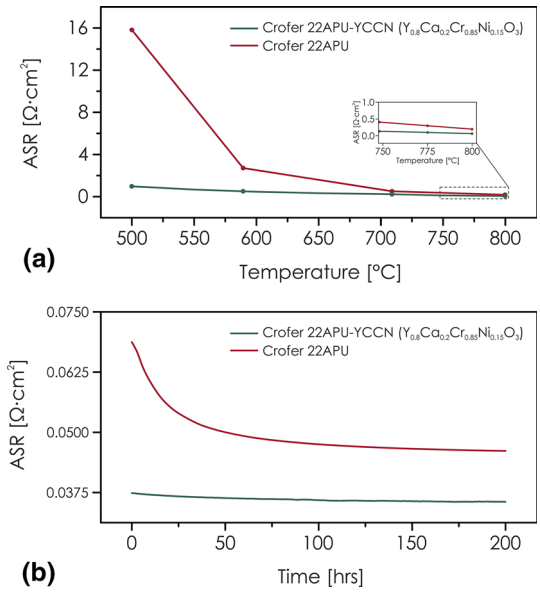

Fig. 9 Value of ASR measured for Crofer 22APU-YCCN layered system in a function of: (a) temperature; (b) time

To examine the suitability of the perovskite coating for the surface modification of ferritic stainless-steel Crofer 22APU in the role of protective–conductive layer for interconnects, measurements of the area-specific resistance (ASR) were taken for two different systems: oxide scale/Crofer 22APU and $Y_{0.8}Ca_{0.2}Cr_{0.85}Ni_{0.15}O_3$ coating/Crofer 22APU. The measurements were taken in the air atmosphere, using a DC 2-probe 4-point method. Based on the measured resistance of the examined systems, their area-specific resistance was calculated from the relation shown in Eq 1.

In Fig. 9(a), a temperature dependence of the determined ASR values for both systems is presented. As it can be seen, in the low-to-medium temperature range (up to 575 °C), the ASR of the scale/uncoated steel system was much higher, although it was quickly decreasing with the increasing temperature. In the case of layer/steel system, the behavior was extremely different, with the ASR being nearly constant within the whole examined temperature range, with only slight decrease in its value in the high temperature range being visible. It should be noted that the ASR of the coated steel was lower than for the uncoated one within the temperature range of interest, although the differences at temperatures higher than 725 °C were very small. At temperature of 800 °C, values of area-specific resistance for both scale/steel and $Y_{0.8}Ca_{0.2}Cr_{0.85}Ni_{0.15}O_3$ layer/steel system were, respectively, 0.037 Ω cm^2 and 0.0368 Ω cm^2.

It is worth mentioning that influence on ASR value has also a number of factors related to physical phenomena, mainly caused by: chemical heterogeneity of the material (oxidant-associated formation of easy conductive paths, diversified microstructure of the material and polarization effects at the phase boundaries).

The values of ASR were also measured at constant temperature of 800 °C in air atmosphere as a function of time. After oxidation for 200 h, results (presented in Fig. 9b) indicated that for the whole duration of measurement, the value was at a constant level of 0.0366 Ω cm^2, which is far below the acceptable limit (0.1 Ω cm^2) (Ref 4).

High potential of the examined coatings for their projected application is confirmed by comparison of the measured ASR values with results obtained for other ceramic/metallic systems dedicated for IT-SOFC applications after similar experimental time (Table 7). The improvement of electrical properties may not look substantial in comparison with the pure scale/Crofer

Table 7 ASR values of various ceramic/metallic layered systems oxidized for different times in air at 800 °C (Ref 26-33)

Layer system	Deposition method	ASR, Ω cm^2	Authors
$Y_{0.8}Ca_{0.2}Cr_{0.85}Ni_{0.15}O_3$/Crofer 22APU	Screen-printing	0.0366	Own research
Scale/Crofer 22APU	…	0.0374	Own research
$La_{0.8}Sr_{0.2}CrO_3$/DIN 50049	Screen-printing	0.09	(Ref 26)
Scale/DIN 50049	…	1.22	(Ref 26)
$Cu_{0.3}Mn_{1.1}Co_{1.8}O_4$/DIN 50049	Screen-printing	0.08	(Ref 27)
$Mn_{1.5}Co_{1.5}O_4$/AL453	Screen-printing	0.0616	(Ref 28)
Scale/AL453	…	0.0993	(Ref 28)
$Y_{0.1}Mn_{1.45}Co_{1.45}O_4$/E-Brite	Screen-printing	0.0076	(Ref 29)
Scale/E-Brite	…	0.0114	(Ref 29)
Co/DIN 50049	Pulsed laser deposition	0.0540	(Ref 30)
Y/DIN 50049	Y-implantation	0.0637	(Ref 31)
La_2O_3/Crofer 22APU	MOCVD	0.05	(Ref 32)
$Mn_{1.5}Co_{1.5}O_4$/Crofer 22APU	PVD	0.004	(Ref 33)

22APU. However, it should be remembered that due to the protective qualities of chemically stable coating, the difference would be much more visible in favor of the $Y_{0.8}Ca_{0.2}Cr_{0.85}Ni_{0.15}O_3$/Crofer 22APU system if longer times of operations were considered. It should also be noted that presented results were obtained using a simple screen-printing method. The appliance of more advanced methods, such as pulsed laser deposition, should allow further improvement of the electrical properties.

4. Conclusions

As a result of the studies, a steel/layer composite system suitable for the application in IT-SOFCs interconnects was created. The first-time application of YCCNs materials in the role of conductive–protective layers for ferritic stainless-steel substrates was proved to be successful. The presented studies allowed selecting the optimal synthesis method, composition and thermal treatment of the perovskites, showing how greatly the properties of these materials can be affected by mentioned factors. The usage of glycine as a chelating agent led to much better final materials, characterized by single-phase structure and good electrical properties.

The usage of cost-effective screen-printing method allowed creating a sufficiently solid layer on the metallic substrate, which exhibited both protective and conductive properties.

Studies of the microstructure and chemical composition by SEM and EDS methods of the cross section of $Y_{0.8}Ca_{0.2}Cr_{0.85}Ni_{0.15}O_3$-Crofer 22APU layered system after oxidation revealed the presence of the additional intermediate layer on the coating/substrate interface.

The electrical properties determined by the ASR (area-specific resistance) measurements are well within the limits for the conductive–protective layers, with the ASR value equal to 0.366 Ω cm^2, even after prolonged annealing.

The fact that the layers proved satisfying despite usage of the rather simple method of deposition suggests that the potential of these materials may be very high, and introduction of more advanced deposition methods such as pulsed laser deposition (PLD) or physical vapor deposition (PVD) may lead to further improvement of their mechanical and electrical properties (i.e., due to the obtaining of thinner, denser layers).

Acknowledgments

The authors would like to express their gratitude to Mr Krzysztof Mroczka from Pedagogical University of Cracow for assistance in SEM–EDS observations. Financial support from the National Science Centre for PRELUDIUM 6 (Grant No. 2013/11/N/ST5/01391) is gratefully acknowledged.

References

1. S.C. Singhal, Solid Oxide Fuel Cells for Stationary, Mobile, and Military Applications, *Solid State Ionics*, 2003, **152–153**, p 405–410
2. J.W. Fergus, Lanthanum Chromite-Based Materials for Solid Oxide Fuel Cell Interconnects, *Solid State Ionics*, 2004, **171**, p 1–15
3. T. Brylewski, M. Nanko, T. Maruyama, and K. Przybylski, Application of Fe-16Cr Ferritic Alloy to Interconnector for a Solid Oxide Fuel Cell, *Solid State Ionics*, 2001, **143**, p 131–150
4. N. Shaigan, W. Qu, D.G. Ivey, and W. Chen, A Review of Recent Progress in Coatings, Surface Modifications and Alloy Developments for Solid Oxide Fuel Cell Ferritic Stainless Steel Interconnects, *J. Power Sources*, 2010, **195**, p 1529–1542
5. K.J. Yoon, J. Stevenson, and O. Marina, Effect of Nickel Substitution on Defect Chemistry, Electrical Properties, and Dimensional Stability of Calcium-Doped Yttrium Chromite, *Solid State Ionics*, 2011, **193**, p 60–65
6. K.J. Yoon, C. Cramer, J. Stevenson, and O. Marina, Advanced Ceramic Interconnect Material for Solid Oxide Fuel Cells: Electrical and Thermal Properties of Calcium- and Nickel-Doped Yttrium Chromites, *J. Power Sources*, 2010, **195**, p 7587–7593
7. K.J. Yoon, J. Stevenson, O. Marina, *Calcium- and Nickel-Doped Yttrium Chromite as an Advanced Ceramic Interconnect Material for Solid Oxide Fuel Cells (SOFCs) (Abstract #1150)* (218th Electrochemical Society Meeting, Las Vegas, 2010)
8. W. Li, M. Gong, and X. Liu, H_2 Oxidation on Doped Yttrium Chromites/Yttrium Stabilized Zirconia Anode of Solid Oxide Fuel Cell, *J. Power Sources*, 2013, **241**, p 494–501
9. S. Wang, B. Lin, Y. Dong, D. Fang, H. Ding, X. Liu, and G. Meng, Stable, Easily Sintered Ca-Zn-Doped $YCrO_3$ as Novel Interconnect Materials for Co-Fired Yttrium-Stabilized Zirconia-Based Solid Oxide Fuel Cells, *J. Power Sources*, 2009, **188**, p 483–488
10. W. Li, M. Gong, and X. Liu, Characterization of Doped Yttrium Chromites as Electrodes for Solid Oxide Fuel Cell by Impedance Method, *J. Electrochem. Soc.*, 2014, **161**, p F551–F560
11. S.W. Paulik, S. Baskaran, and T.R. Armstrong, Mechanical Properties of Calcium-Substituted Yttrium Chromite, *J. Mater. Sci. Lett.*, 1999, **18**, p 819–822
12. T. Armstrong, J. Stevenson, D. McCready, S. Paulik, and P. Raney, The Effect of Reducing Environments on the Stability of Acceptor Substituted Yttrium Chromite, *Solid State Ionics*, 1996, **92**, p 213–223
13. J. Stevenson, B. Koeppel, *FY13 Annual Progress Report for SECA Core Technology Program*, Prepared for the U.S. Department of Energy under Contract DE-AC05-76RL01830, Washington, 2013)
14. Y. Jianyi, *Practical Approach to Characteristic Reaction Sintering with Ceramics $Y_{0.7}Ca_{0.3}Cr_{0.9}Zn_{0.1}O_3$ and $Y_{0.8}Ca_{0.2}Cr_{0.85}Ni_{0.15}O_3$*, Master thesis (Kunshan University of Science and Technology, Taiwan, 2012). Accessed 10 Jan 2018. http://ir.lib.ksu.edu.tw/handle/987654321/16305
15. C. Seokgon, *Doping Effect of Fe, Co or Ni on YCC($Y_{0.75}Ca_{0.25}CrO_{3-\delta}$) Perovskites as the SOFC Interconnect*, PhD thesis (Pohang University of Science and Technology, South Korea, 2011). Accessed 10 Jan 2018. http://oasis.postech.ac.kr/handle/2014.oak/1114
16. M. Stygar, K. Matsuda, S. Lee, and T. Brylewski, Corrosion Behavior of Crofer 22APU for Metallic Interconnects in Single and Dual Atmosphere Exposures at 1073 K, *Acta Phys. Pol. A*, 2017, **131**, p 1394–1398
17. M. Stygar, T. Brylewski, A. Kruk, and K. Przybylski, Oxidation Properties of Ferritic Stainless Steel in Dual Ar–H_2–H_2O/Air Atmosphere Exposure with Regard to SOFC Interconnect Application, *Solid State Ionics*, 2014, **262**, p 449–453
18. M. Stygar, J. Dąbrowa, P. Dziembaj, and T. Brylewski, Influence of Gaseous Media Flow in the Dual Ar-H_2-H_2O/Air Atmosphere Setup on the Scale Growth Kinetics of Crofer 22APU Ferritic Stainless Steel, *J. Mater. Eng. Perform.*, 2017, **26**, p 540–546
19. K. Huang, P.Y. Hou, and J.B. Goodenough, Characterization of Iron-Based Alloy Interconnects for Reduced Temperature Solid Oxide Fuel Cells, *Solid State Ionics*, 2000, **129**, p 237–250
20. S. Chevalier, G. Caboche, K. Przybylski, and T. Brylewski, Effect of Nano-Layered Coatings on the Electrical Conductivity of Oxide Scale Grown on Ferritic Steels, *J. Appl. Electrochem.*, 2009, **39**, p 529–534
21. P. Scherrer, Bestimmung der Grösse und der Inneren Struktur von Kolloidteilchen Mittels Röntgenstrahlen, Nachrichten von der Gesellschaft der Wissenschaften zu Göttingen, *Mathematisch-Physikalische Klasse*, 1918, **1918**, p 98–100

22. S. Degterov and A.D. Pelton, Critical Evaluation and Optimization of the Thermodynamic Properties and Phase Diagrams of the CrO-Cr_2O_3, CrO-Cr_2O_3-$A1_2O_3$, and CrO-Cr_2O_3-CaO Systems, *J. Phase Equilib.*, 1996, **17**, p 476–487
23. J.P.R. de Villiers and A. Muan, Liquidus-Solidus Phase Relations in the System CaO-CrO-Cr_2O_3-SiO_2, *J. Am. Ceram. Soc.*, 1992, **75**(6), p 1333–1341
24. T. Brylewski, W. Kucza, A. Adamczyk, A. Kruk, M. Stygar, M. Bobruk, and J. Dąbrowa, Microstructure and Electrical Properties of $Mn_{1+x}Co_{2-x}O_4$($0 <= x <= 1.5$) Spinels Synthesized Using EDTA-Gel Processes, *Ceram. Int.*, 2014, **40**, p 13873–13882
25. K. Przybylski, T. Brylewski, and J. Morgiel, Interfacial Interactions Between Some La-Based PerovskiteThick Films and Ferritic Steel Substratewith Regard to the Operating Conditions of SOFC, *Mater. Sci. Forum*, 2004, **461–464**, p 1099–1106
26. T. Brylewski, J. Dąbek, K. Przybylski, J. Morgiel, and M. Rękas, Screen-Printed (La, Sr)CrO_3 Coatings on Ferritic Stainless Steel Interconnects for Solid Oxide Fuel Cells Using Nanopowders Prepared by Means of Ultrasonic Spray Pyrolysis, *J. Power Sources*, 2012, **208**, p 86–95
27. T. Brylewski, A. Kruk, M. Bobruk, A. Adamczyk, J. Partyka, and P. Rutkowski, Structure and Electrical Properties of Cu-Doped Mn-Co-O Spinel Prepared Via Soft Chemistry and Its Application in Intermediate-Temperature Solid Oxide Fuel Cell Interconnects, *J. Power Sources*, 2016, **333**, p 145–155
28. A. Kruk, M. Stygar, and T. Brylewski, Mn–Co Spinel Protective–Conductive Coating on AL453 Ferritic Stainless Steel for IT-SOFC Interconnect Applications, *J. Solid State Electrochem.*, 2013, **17**, p 993–1003
29. A. Kruk, M. Stygar, M. Krauz, M. Homa, A. Adamczyk, W. Kucza, P. Rutkowski, M. Bobruk, A. Gil, and T. Brylewski, Microstructure and Electrical Properties of a Spinel Coatings on Selected Ferritic Stainless Steels, *Ceram. Mater.*, 2014, **67**, p 235–244 ((in polish))
30. A. Kruk, A. Adamczyk, A. Gil, S. Kąc, J. Dąbek, M. Ziąbka, and T. Brylewski, Effect of Co Deposition on Oxidation Behavior and Electrical Properties of Ferritic Steel for Solid Oxide Fuel Cell Interconnects, *Thin Solid Films*, 2015, **590**, p 184–192
31. T. Brylewski, A. Gil, A. Rakowska, S. Chevalier, A. Adamczyk, J. Dąbek, A. Kruk, M. Stygar, and K. Przybylski, Improving the Physicochemical Properties of Fe-25Cr Ferritic Steel for SOFC Interconnects Via Y-Implantation and Y_2O_3-Deposition, *Oxid. Met.*, 2013, **80**, p 83–111
32. P. Piccardo, P. Gannon, S. Chevalier, M. Viviani, A. Barbucci, G. Caboche, R. Amendola, and S. Fontana, ASR Evaluation of Different Kinds of Coatings on a Ferritic Stainless Steel as SOFC Interconnects, *Surf. Coat. Technol.*, 2007, **202**, p 1221–1225
33. V.I. Gorokhovsky, P.E. Gannon, M.C. Deibert et al., Deposition and Evaluation of Protective PVD Coatings on Ferritic Stainless Steel SOFC Interconnects, *J. Electrochem. Soc.*, 2006, **153**, p A1886–A1893